DOI: 10.61782/fa.2023.0399

forum acusticum 2023

TOWARDS AN ACTIVE SEMI-ANECHOIC ROOM: SIMULATIONS AND FIRST MEASUREMENTS

Cédric Pinhède[1*] **Romain Boulandet**[2] **Emmanuel Friot**[1]
Mark R. Allado[2] **Renaud Côte**[1] **Philippe Herzog**[3]
[1] Aix Marseille Univ, CNRS, Centrale Marseille, LMA UMR7031, Marseille, France
[2] University of Applied Sciences and Arts Western Switzerland, Geneva, Switzerland
[3] ARTEAC-LAB, Marseille, France

ABSTRACT

Semi-anechoic rooms are used for the acoustic characterization of noise sources. They involve heavy infrastructures and thick absorbent lining. The purpose of the ongoing project "DADA" (Dôme Anti-Diffraction Acoustique) is to demonstrate a lower-cost alternative by supplementing a thin passive lining with active technology. This project targets an actual size functional demonstrator, an important milestone before tackling a fully active anechoic room at the Laboratory of Mechanics and Acoustics (LMA). Previous work has achieved the active reduction of the pressure scattered by the reflective wall of a semi-anechoic room, in the $80 - 200$ Hz frequency band. These results validated an innovative approach allowing to control the scattered pressure throughout the measurement volume, using a setup located over its periphery. The DADA project extends these results by dealing with the five non-reflecting walls of a semi-anechoic room. Analytical and FEM simulations are described and discussed. They allow a parametric study of many design aspects, including the structure of the active control system and transducers locations. The resulting design will be presented, together with simulations able to deal with test sources of increasing complexity.

Keywords: *Semi-Anechoic room, Active noise control, Acoustical measurements, Active Anechoicity*

**Corresponding author*: *pinhede@lma.cnrs-mrs.fr.*

1. INTRODUCTION

The principle of active anechoicity consists in cancelling the acoustic reflections of the walls of a room with the help of an active system. The strategy for controlling the acoustic field scattered by the walls is based on the fact that a unique linear operator maps the total acoustic field close to the walls to the field scattered by these walls, whatever the direct acoustic field is [1–3]. This "scattering operator" can be identified from off-line measurements involving known direct fields and then used to calculate the scattered sound field caused by an unknown direct field. An actuator array is then used to minimize this scattered sound field, just like an "ordinary" total sound field picked up by microphones.

A recent PhD work allowed to cloak the reflective wall of a semi-anechoic room acoustically in the $80 - 200$ Hz frequency band. The DADA project proposed here targets a more useful situation for acoustic measurements, aiming at suppressing the acoustic scattering by five walls. The objective of the project is to produce a functional demonstrator with dimensions ($W = 4.5$ m; $D = 3.65$ m; $H = 3$ m) compatible with industrial applications. Fig. 1 describes the principle of the demonstrator to be realized.

2. THE SCATTERED FIELD CONTROL STRATEGY APPLIED TO ACTIVE SEMI-ANECHOIC

The aim of the strategy is to transform by active control a room with a reflective floor Γ' into a low-frequency semi-anechoic room, see Fig. 1. For this purpose, the control sources are installed behind a surface Γ over which mi-

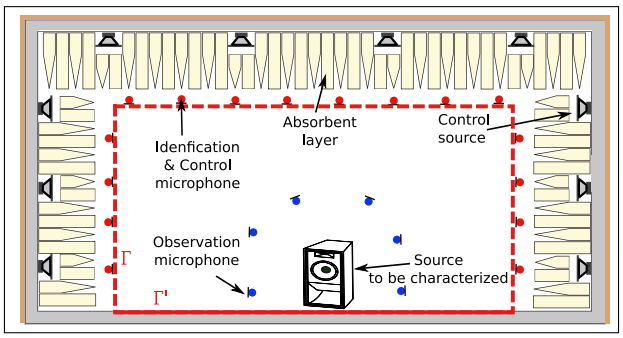

Figure 1. Principle of a semi-anechoic room with active technology.

crophones are placed, allowing to estimate and control the field scattered by the walls.

A major advantage of this geometry is that the installation of the microphones close to the reflecting walls naturally places these microphones close to the antinodes of the first acoustic modes, avoiding the homogeneous Dirichlet conditions that would defeat the control strategy. A fine-tuning phase may require a few additional microphones sensitive to possible modes that are otherwise indistinguishable.

2.1 Integral formulation of the scattered pressure

For a distribution of f sources in the volume, the sound pressure in the volume can be written at the ω pulsation, using *any* Green's function G [4, p. 321] for the Helmholtz equation :

$$\begin{aligned} p_{tot}(\mathbf{r},\omega) &= \int_V f(\mathbf{r}_0,\omega) G(\mathbf{r}|\mathbf{r}_0,\omega) dV_0 \\ &+ \int_{\Gamma+\Gamma'} \left[G(\mathbf{r}|\mathbf{r}_0,\omega) \frac{\partial}{\partial n_0} p(\mathbf{r}_0,\omega) \right. \\ &\left. - p(\mathbf{r}_0,\omega) \frac{\partial}{\partial n_0} G(\mathbf{r}|\mathbf{r}_0,\omega) \right] d\Gamma_0 \end{aligned} \tag{1}$$

Chosing a Green function $\hat{G}$ which respects the acoustic boundary conditions on Γ', the surface integral cancels on Γ' and the direct field and the one scattered by the walls behind Γ may be respectively defined by :

$$p_{dir}(\mathbf{r},\omega) = \int_V f(\mathbf{r}_0,\omega) \hat{G}(\mathbf{r}|\mathbf{r}_0,\omega) dV_0 \tag{2}$$

$$\begin{aligned} p_{sca}(\mathbf{r},\omega) = \int_\Gamma & \hat{G}(\mathbf{r}|\mathbf{r}_0,\omega) \frac{\partial}{\partial n_0} p(\mathbf{r}_0,\omega) \\ & - p(\mathbf{r}_0,\omega) \frac{\partial}{\partial n_0} \hat{G}(\mathbf{r}|\mathbf{r}_0,\omega) \; d\Gamma_0 \end{aligned} \tag{3}$$

The field scattered by the walls depends linearly on the total pressure on Γ and its normal gradient. This function is thus independent of the sources located in the volume.

2.2 Substitution of the normal gradient term

Active control preferably relies on sound pressure measurements which are easier to obtain and more robust than pressure gradients measurements. Assuming that the walls have a localized behaviour and can be described by a specific wall admittance β, and that the microphones are placed on the walls, then on Γ :

$$\frac{\partial}{\partial n_0} p(\mathbf{r}_0,\omega) = -ik\beta p(\mathbf{r}_0,\omega) \tag{4}$$

The diffracted pressure is then written as a surface integral involving only the total pressure. Γ may then be discretized, ensuring to have at least two pressure sensors per wavelength. The integral can thus be approximated by a discrete sum :

$$p_{sca}(\mathbf{r},\omega) \approx \sum_k g_k(\mathbf{r},\omega) p_k(\mathbf{r}_k,\omega) \tag{5}$$

The key advantage of this representation is that the filters $g_k(\mathbf{r})$ are independent of the noise sources in the volume. This approximation is widely valid although it is difficult to establish under what exact conditions when the acoustic reflection on Γ cannot be modelled by a local surface impedance [3]. In the case of DADA, it is in particular not valid at the "irregular" frequencies corresponding to the resonances of the $p = 0$ boundary problem on Γ. To circumvent this problem, it may suffice to move or add some microphones outside Γ (*cf.* § 3.4) .

2.3 Identification of scattering filters and control

The coefficients of the above approximation may be determined through an off-line identification. This requires to know the scattered (or direct) and total fields for a number of source distributions and to solve the associated linear inverse problem. One possible mean is to move a "reference source" of known radiation pattern into the volume to generate the necessary data [5], taking into account the image field generated by the ground. Then a classic control is applied to cancel the estimated scattered pressure.

3. DADA SIMULATIONS

This section presents the analytical modeling of the Active Anti-Diffraction Dome with weakly absorbing walls.

3.1 Analytical modelling

The primary and control sources are considered as acoustic monopoles. The transfer matrix between the source volume velocity and the cavity pressure is calculated from the known expression of the rigid cavity Green's function in which modal damping rates ξ_n are introduced to take into account the effect of the absorber.

The acoustic Green's function G initially derived from a hard wall cavity model is expressed as a series of damped modes :

$$G(\boldsymbol{r}, \mathbf{r}_0) = \sum_{n=0}^{+\infty} \frac{\boldsymbol{\psi}_n^t(\mathbf{r})\boldsymbol{\psi}_n(\mathbf{r}_0)}{(k_n^2 + 2j\xi_n k_n k - k^2)\int_V \boldsymbol{\psi}_n^2 dV} \quad (6)$$

where the $\boldsymbol{\psi}_n$ are eigenmodes and $f_n = \frac{c}{2\pi}k_n$, with c the celerity of sound, the resonance frequencies of the cavity.

In a parallelepipedic (3D) cavity, the eigenmodes are products of cosine function of the space variables. In this way the Green's function takes on a finite value at resonant frequencies. The damping rates to be used for a given cavity may be derived from a Finite Element Model (FEM) of the cavity lined with absorbing material.

Using this Green's function, at each pulsation ω, the pressure p produced at a point $\boldsymbol{r}$ of the cavity by a monopole at the point $\mathbf{r}_0$ providing a volume q of fluid (i.e. of volume velocity $\dot{q} = j\omega q$) is finally written (with ρ designating the density of the fluid) :

$$p(\boldsymbol{r}, \mathbf{r}_0) = -\rho c^2 \omega^2 q \sum_{n=0}^{+\infty} \frac{\boldsymbol{\psi}_n^t(\mathbf{r})\boldsymbol{\psi}_n(\mathbf{r}_0)}{(\omega_n^2 + 2j\xi_n\omega_n\omega - \omega^2)\int_V \boldsymbol{\psi}_n^2 dV} \quad (7)$$

This way, it is possible to calculate the pressure generated at any point in the room, for a source considered as a monopole.

3.2 Scattered pressure control

Let $\mathbf{p}_{sca}$ be the field scattered by the upper walls of the room at the minimization points when the primary source is in operation. Let $\mathbf{C}$ be the transfer matrix between the control sources and the pressure at the same minimization points. The vector $\mathbf{u}$ of commands, to be supplied to the control sources for control, must minimize at each frequency the criterion :

$$J = \|\mathbf{p}_{sca} + \mathbf{C}\mathbf{u}\|^2 \quad (8)$$

Note that for the actual facility, this control might be performed in real time, using an algorithm close to the *Filtered-Error LMS* [2, 6, p. 251]. This would even allow to integrate the filtering of pressures on Γ with very little additional CPU cost.

3.3 Configuration of the simulation

In a rigid cavity of dimensions 4.5 m x 3.65 m x 3 m, 802 modes exhibit a resonance frequency below 500 Hz.

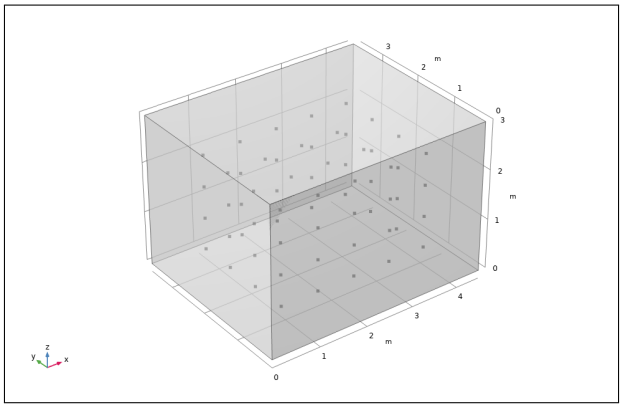

Figure 2. Location of the 62 minimization points.

Fig. 2 shows the modelled room and the positions of the 62 minimization points uniformly distributed over a closed surface surrounding the control volume. Before applying the control, the identification phase requires the calculation of all transfers between the minimization points and the identification sources located in the control volume Fig. 3.

In a first step, analytical simulations based on the modal series for a 2D model allowed to analyze the main parameters of the setup and to choose a suitable configuration.

3.4 Results from 2D simulations

In a previous paper [7], 2D simulations were performed in the $20 - 400$ Hz range with 102 modes. The modal damping rates used in the analytical model were derived from a

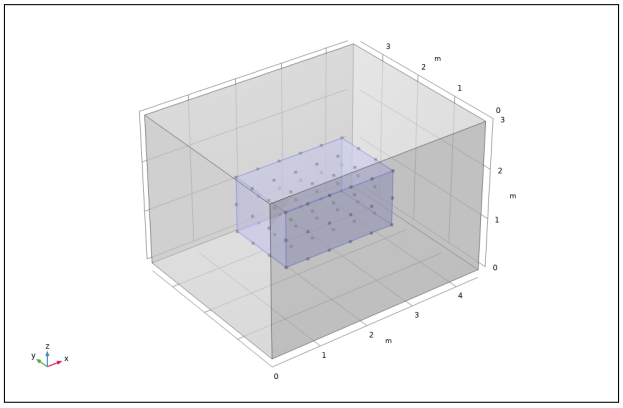

Figure 3. Location of the 72 identification sources distributed within the control volume (in blue).

FEM model of the cavity considering a 2% absorption coefficient with purely reel impedance, over the upper walls; these rates account for the dissymmetry of the absorption. This FEM model also provides a better representation of the near field of a real source (enclosure) and the effect of a given absorbing material.

These previous results show that the identification of the scattering filter is correct and allows to estimate the scattered pressure at the minimization points. In addition, a comparison of two control strategies is performed: one consists in cancelling the scattered pressure in the measurement zone and the other at the walls. The performance of the wall control is comparable to that obtained in the measurement zone with the exception of additional accidents. Indeed, the pressure control on a line does not allow to cancel the pressure in the surface at the resonance frequencies of the p = 0 boundary problem on Γ. Without additional microphones this problem is largely mitigated in practice by breaking the symmetry of the minimization points. In contrast to the control of the scattered pressure in the measurement zone, the control near the wall allows the global cancellation of the scattered pressure.

4. 3D MODELING OF THE ACTIVE SEMI-ANECHOIC ROOM

4.1 Configuration

3D simulations are then run using LiveLink™ for MATLAB® which provides a direct connection to MATLAB® while running COMSOL Multiphysics® 5.6. The room is modelled as a rectangular parallelepiped of dimension $4.5 \times 3.65 \times 3$ m^3 using the physics *pressure acoustics, frequency domain*. An impedance condition of 8.10^4 Pa.s/m is applied to all walls. The mesh is controlled by the physics of the model taking into account the maximum wavelength of the simulation.

The simulations are performed over the $20 - 200$ Hz frequency range in 1 Hz steps and stored in a matrix of dimensions $62 \times 181 \times 72$. Fig. 4 shows the pressure levels calculated at several minimization points when the room is excited by one of the monopoles.

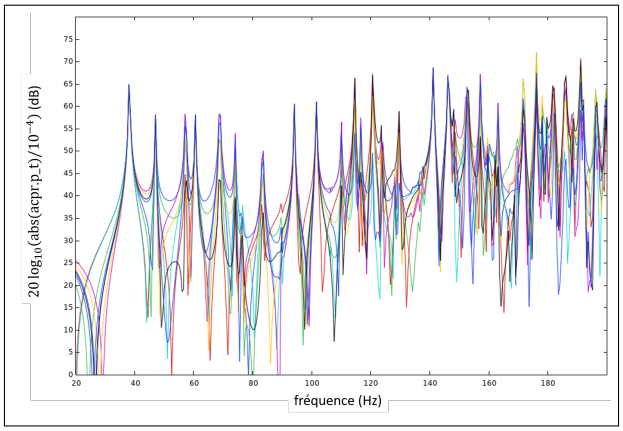

Figure 4. Pressure level at the 8 minimization points located in the vertical plane at $x = 0.7$ m.

4.2 Identification step of the scattering filter

The identification sources in the measurement volume are modelled by monopoles with flow rate $q_0 = 10^{-4}$ m^3/s. For the identification step of the scattering filter, the direct pressures p_{dir} are calculated at each identification microphone (MicID) position by considering the radiation of the monopole in a half-space closed by a perfectly-matched layer (PML). The floor is modelled as a acoustic hard boundary, see Fig. 5. This is done for each position of the identification source (SourceID).

The total pressures p_{tot} are calculated the same way but in the rectangular room with boundary specific impedance condition of $198\rho c$ which leads to 2% absorption applied to all walls, see Fig. 6. Then, the exact scattered pressures p_{sca} are deduced from p_{dir} and p_{tot} as:

$$p_{sca} = p_{tot} - p_{dir} \tag{9}$$

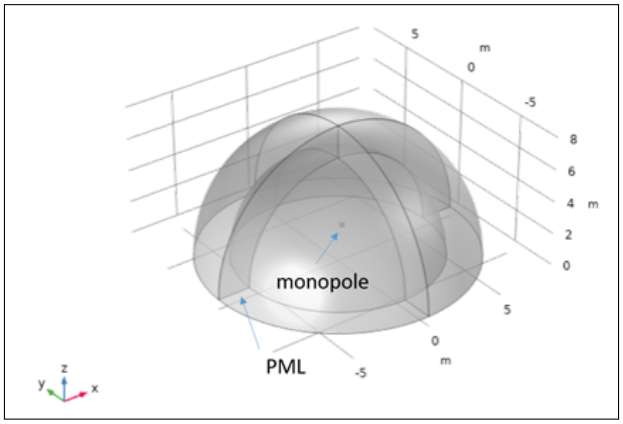

Figure 5. Radiation of a monopole in a half-space.

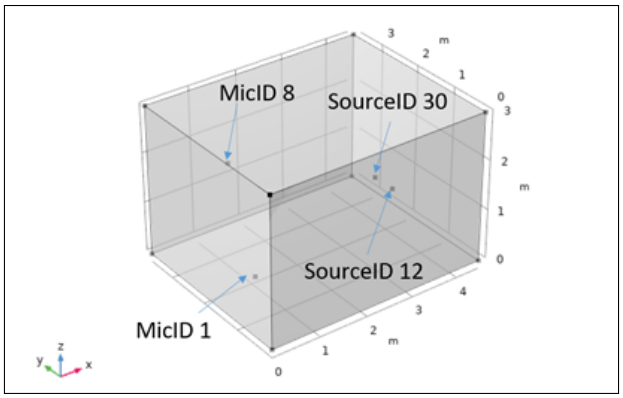

Figure 6. Source (number 12, 30) and microphone (number 1, 8) identification positions.

The identification of the scattering filter is obtained by solving Eqn. (5) from this dataset, see details in [5].

4.3 Control of the scattered pressure

The control is performed on the identification microphones used previously to identify the scattering filter. The control sources are modelled as plane pistons positioned over the walls of the room, see Fig. 7.

They are actuated successively by applying an acceleration

$$a = j * \omega * q_0 / S \tag{10}$$

where $S = 0.0133$ m^2 is the surface area of each piston. The resulting pressure is evaluated for all the minimization microphone positions to generate the transfer matrix **C** with the control sources at each frequency. The

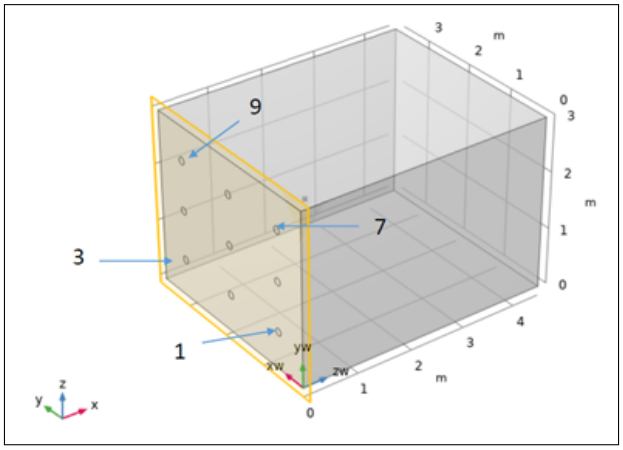

Figure 7. positions of control sources 1 to 9.

commands **u** to be supplied to the control sources are obtained by solving Eqn. (8).

4.4 Control Results

Once the transfer matrix for driving all the control sources has been obtained it is used to implement the active control of the scattered field produced by a test source. As an illustration, we used the monopole sourceID 12 and sourceID 30 as test source and we observed the resulting pressure at the identification microphones (MicID 1 and 8) with control on using an exact (legend P_{on} exact) vs an estimated (legend P_{on} estimated) formulation. In the following illustrations, the legend P_{dir} corresponds to the radiation from the test source in a half-space closed by a PML and the legends P_{tot} and P_{sca} correspond to the radiations from the test source in the room with specific impedance conditions at the boundaries (*cf.* § 4.2).

Fig. 8 illustrates the frequency response of the room between 20 Hz and 200 Hz without and with active control when the test source (SourceID 30) is activated only and resulting pressure is computed at microphone MicD 1. The control result is effective up to 180 Hz. The pressure obtained with control is close to the direct pressure with reductions of several tens of decibel, up to 30 dB at 37 Hz. In addition, the identification of the scattering filter is correct: the control results using the exact or estimated scattered pressure are almost equivalent.

Fig. 9 shows the frequency response of the room, in the same configuration as seen previously, but with the

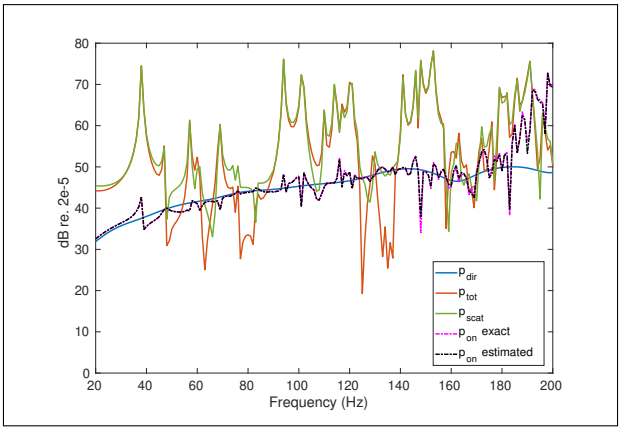

Figure 8. Pressure with and without control on microphone MicD 1 for the test source SourceID 30.

SourceID 12 test source and the MicID 8 microphone. The results of the control are similar to those obtained previously except for an accident around 120 Hz. The loss of controllability at this frequency could be due to the particular arrangement of the transducers. A response dip which is still being investigated

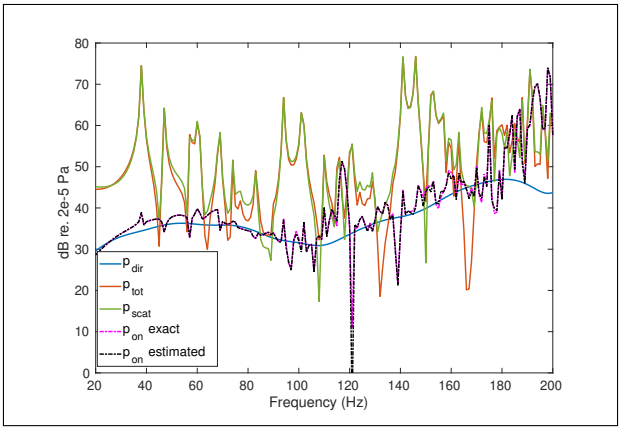

Figure 9. Pressure with and without control on microphone MicD 8 for the test source SourceID 12.

The following illustrations show the distribution of the acoustic pressure in the room computed at 38 Hz and 47 Hz with the control switched off or on. Only the exact scattered pressure is used for control.

The left-side Fig. 10 shows, at 38 Hz, the pressure distribution without control corresponds to the 1-0-0 mode. The right-side Fig. 10 shows that the modal pressure distribution disappears with control. The pressure is significantly reduced on the walls and especially on the floor. The amplitudes of the control sources located at the corners (pressure antinode) are greater than those distributed closer to the center of the room (pressure node).

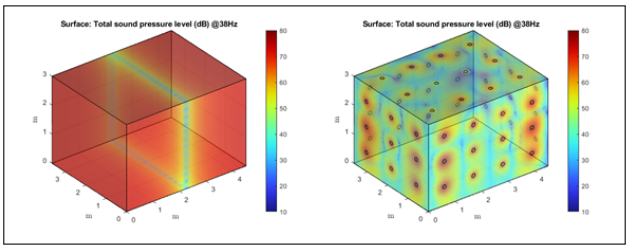

Figure 10. Distribution of the acoustic pressure at 38 Hz, without control (left side) and with control (rigth side).

The left-side Fig. 11 shows, at 47 Hz, the pressure distribution without control corresponds to the 0-1-0 mode. The right-side Fig. 10 shows that the modal pressure distribution again disappears with control. As for the results at 38 Hz, the pressure is significantly reduced on the walls and especially on the floor. The amplitudes of the control sources located near the hard floor have a lower contribution to the 0-1-0 mode compared to the 1-0-0 mode.

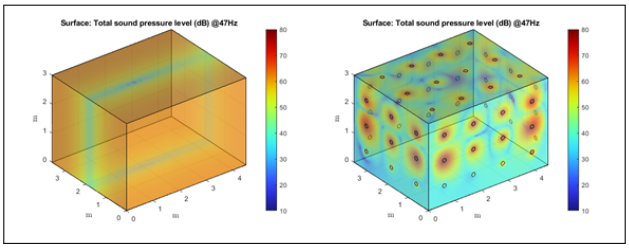

Figure 11. Distribution of the acoustic pressure at 47 Hz, without control (left side) and with control (rigth side).

The above results show that the simulated control is quite satisfactory. They also validate the simulation procedure, involving FEM computations in COMSOL®, performed by HEPIA, and signal processing in MATLAB®, performed by LMA. This remote collaboration has proven to be effective and will allow the design and tuning of the DADA facility.

5. EXPERIMENTATION

A demonstrator ($W = 5.33$ m, $D = 4.22$ m, $H = 2.73$ m) is under construction at LMA. The walls of the room are made of a sandwich concept consisting in a dual inner layer of plasterboard, a layer of absorbent material and a single outer layer of plasterboard. The walls and floor have been painted and the opening has a dual door. A Truss structure is installed in order to hold the devices of the control system composed of loudspeakers and microphones, see Fig. 12.

Figure 12. The demonstrator DADA.

The first measurements were made in this room with a source built at the LMA. A model of this source was developed in order to estimate the pressure at a point in the room from the internal pressure measurement, see details in [8]. The source was located at one corner near the floor and the microphone was located at the opposite corner near the ceiling. The pressure level normalized by the direct pressure of the source between $20 - 200$ Hz is shown in Fig. 13.

Resonances below 100 Hz are less pronounced than those observed in simulation (see Fig. 4), probably because plasterboard is more absorbent than a rigid wall.

6. CONCLUSION

A previous 2D analytical model has shown the potential for active control of the diffracted field in the wall via the prior identification of scattering filters and the dissymmetrization of the minimization point positions. The present 3D FEM model allows a more accurate and realistic simulation, leading to the optimization of the active control setup. The realization of the demonstrator is launched in parallel at the LMA.

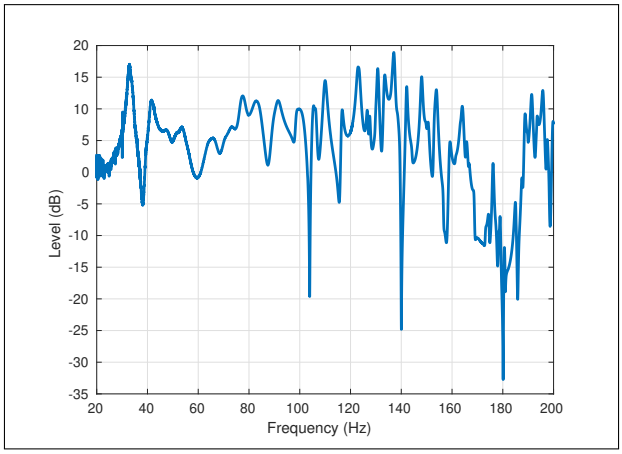

Figure 13. Frequency response in the DADA room.

7. ACKNOWLEDGMENTS

This work received support from the French government under the France 2030 investment plan, as part of the Initiative d'Excellence d'Aix-Marseille Université - A*MIDEX (AMX-19-IET-010)

8. REFERENCES

[1] E. Friot, R. Guillermin, and M. Winninger, "Active control of scattered acoustic radiation: a real-time implementation for a three-dimensional object," *Acta Acustica united with Acustica*, vol. 92, pp. 278–288, 2006. Publisher: Hirzel Verlag.

[2] E. Friot, "Control of low-frequency wall reflections in an anechoic room," in *ACTIVE 2006*, (Australia), pp. CD–ROM (9 pages), Australian Acoustical Society, 2006.

[3] D. Habault, E. Friot, P. Herzog, and C. Pinhède, "Active control in an anechoic room : Theory and first simulations," *Acta Acustica united with Acustica*, vol. 103, pp. 369–378, May 2017. Publisher: Hirzel Verlag.

[4] P. M. Morse and K. U. Ingard, *Theoretical Acoustics*. Princeton University Press, 1986. Google-Books-ID: KIL4MV9IE5kC.

[5] C. Pinhède, D. Habault, E. Friot, and P. Herzog, "Active control of the field scattered by the rigid wall of a semi-anechoic room—Simulations and full-scale off-line experiment," *Journal of Sound and Vibration*, vol. 506, p. 116134, Aug. 2021.

[6] S. Elliott, *Signal Processing for Active Control*. Jan. 2001.

[7] C. Pinhède, M. Allado, R. Boulandet, R. Cote, E. Friot, and P. Herzog, "Simulations d'un dispositif de semi-anéchoïcité active," in *16ème Congrès Français d'Acoustique, CFA2022*, (Marseille, France), Société Française d'Acoustique and Laboratoire de Mécanique et d'Acoustique, Apr. 2022.

[8] C. Pinhède and P. Herzog, "Design and measurement of a reference source at lower frequencies," in *Forum Acusticum*, (Lyon, France), pp. 3365–3372, Dec. 2020.